SPACE TELESCOPE SCIENCE INSTITUTE
Operated for NASA by AURA

Instrument Science Report WFC3 2005-002

Results of WFC3 Thermal Vacuum Testing - UVIS Channel Throughput

T.M. Brown & I.N. Reid
February 3, 2005

ABSTRACT

The throughput measurements for the WFC3 UVIS channel, taken during the Fall 2004 thermal-vacuum test, show that the UVIS throughput is excellent, meeting or exceeding expectations at most wavelengths. These measurements were obtained through both the "clear" aperture and through a subset of the broad-band UVIS filters. The clear throughput was obtained on each detector chip, scanning a monochromatic source from the near-UV (200 nm) to the near-IR (1000 nm). The filtered throughput was obtained at one field point using a monochromatic source at the central wavelength of each tested filter.

Throughput Tests

The Fall 2004 thermal vacuum test for WFC3 was the first to characterize the fully-assembled instrument, housing both the UVIS and IR channels. This report focuses on the results of the throughput measurements made on the UVIS channel, through both the "clear" aperture and through a subset of the UVIS filters. The results are compared to the expected throughput, which is based upon the product of all measured component throughputs (Brown, T.M. 2003, ISR WFC3-2003-13).

Settings for both the optical stimulus (CASTLE) and the WFC3 are summarized in Tables 1 (clear) and 2 (filtered). All tests were done with a 200 micron fiber on the optical stimulus, projecting a spot roughly 20 pixels wide on the WFC3 CCD, thus averaging over pixel-to-pixel variations in response and allowing measurements with a high signal-to-noise ratio without approaching saturation. Tests of chip 1 throughput used the UV16 field point (roughly centered in the upper left-hand quadrant), while tests of chip 2 throughput used the UV15 field point (roughly centered in the lower left-hand quadrant). Clear throughputs were measured on chips 1 and 2, but filtered throughputs were measured on chip 2 only. Note that in the FITS files produced by the STScI pipeline, confusingly, chip 1 data are stored in extension [SCI,2] and chip 2 data are stored in extension [SCI,1]. The throughput images were taken in an 800x800 pixel subarray roughly centered on the relevant field point.

Table 1: Optical stimulus and WFC3 settings for clear throughput measurements

stimulus wavelength (nm)	Bandpass (nm)	stimulus lamp	stimulus fiber	stimulus mono-chromator	stimulus ND	WFC3 exposure time (sec)
200	5	Xenon	UV	Double UV	none	100
205	5	Xenon	UV	Double UV	none	30
210	5	Xenon	UV	Double UV	none	10
215	5	Xenon	UV	Double UV	none	5
220	5	Xenon	UV	Double UV	ND1	40
225	5	Xenon	UV	Double UV	ND1	20
230	5	Xenon	UV	Double UV	ND1	10
235	5	Xenon	UV	Double UV	ND1	7
240	5	Xenon	UV	Double UV	ND1	5
245	5	Xenon	UV	Double UV	ND1	4
250	5	Xenon	UV	Double UV	ND1	3
255	5	Xenon	UV	Double UV	ND1	2
260	5	Xenon	UV	Double UVIS	ND1	2
270	5	Xenon	UV	Double UVIS	ND1	1
280	5	Xenon	UV	Double UVIS	ND1	1
290	5	Xenon	UV	Double UVIS	ND2	10
300	5	Xenon	UV	Double UVIS	ND2	5
320	5	Xenon	UV	Double UVIS	ND2	3
340	5	Xenon	UV	Double VIS	ND3	1
360	5	Xenon	UV	Double VIS	ND3	10
380	5	Xenon	UV	Double VIS	ND3	8
400	5	Xenon	UV	Double VIS	ND3	8
450	5	Xenon	UV	Double VIS	ND3	5
500	5	Xenon	UV	Double VIS	ND3	8
550	5	Xenon	UV	Double VIS	ND3	8
600	5	Xenon	UV	Double VIS	ND3	10
650	10	Xenon	UV	Double VIS	ND3	10
700	10	Xenon	UV	Double VIS	ND3	20
750	10	Tungsten	VISIR	Double IR	ND2	10
800	10	Tungsten	VISIR	Double IR	ND2	5
850	10	Tungsten	VISIR	Double IR	ND2	3
900	10	Tungsten	VISIR	Double IR	ND3	10
950	10	Tungsten	VISIR	Double IR	ND3	10
1000	10	Tungsten	VISIR	Double IR	ND3	10

Table 2: Optical stimulus and WFC3 settings for filtered throughput measurements

WFC3 filter[a]	Bandpass (nm)	stimulus lamp	stimulus fiber	stimulus mono-chromator	stimulus ND	WFC3 exposure time (sec)
F218W	10	Xenon	UV	Double UV	none	7
CLEAR	10	Xenon	UV	Double UV	none	2
F225W	10	Xenon	UV	Double UV	none	3
CLEAR	10	Xenon	UV	Double UV	none	1
F275W	10	Xenon	UV	Double UV	ND1	3
CLEAR	10	Xenon	UV	Double UV	ND1	1
F300X	10	Xenon	UV	Double UV	ND1	1
CLEAR	10	Xenon	UV	Double UV	ND2	5
F336W	10	Xenon	UV	Double UV	ND2	2
CLEAR	10	Xenon	UV	Double UV	ND2	2
F390W	10	Xenon	UV	Double UV	ND2	1
CLEAR	10	Xenon	UV	Double UV	ND2	1
F438W	10	Xenon	UV	Double UVIS	ND2	1
CLEAR	10	Xenon	UV	Double UVIS	ND2	1
F475X	10	Xenon	UV	Double UVIS	ND3	5
CLEAR	10	Xenon	UV	Double UVIS	ND3	5
F475W	10	Xenon	UV	Double UVIS	ND3	5
CLEAR	10	Xenon	UV	Double UVIS	ND3	5
F555W	10	Xenon	UV	Double VIS	ND2	1
CLEAR	10	Xenon	UV	Double VIS	ND2	1
F606W	10	Xenon	UV	Double VIS	ND2	1
CLEAR	10	Xenon	UV	Double VIS	ND2	1
F625W	10	Xenon	UV	Double VIS	ND2	1.5
CLEAR	10	Xenon	UV	Double VIS	ND2	1
F775W	10	Xenon	VISIR	Double IR	ND2	1
CLEAR	10	Xenon	VISIR	Double IR	ND2	1
F814W	12	Tungsten	VISIR	Double IR	ND2	5
CLEAR	12	Tungsten	VISIR	Double IR	ND2	5

a. Note that the optical stimulus was set to the central wavelength of the filter for the exposure through the filter and the subsequent exposure taken through the clear aperture. For example, the first two exposures were taken at 218 nm, the next two at 225 nm, etc.

The clear throughput measurements were taken as a pair of exposures at each wavelength, with identical settings, to look for drift in the output of the optical stimulus. The drift was minimal, and the count rates consistently agreed to better than 1%. The filtered throughput measurements were also taken as pairs of measurements at each wavelength, but with distinct settings: one through the filter at the filter's central wavelength, followed by one through the clear aperture at the same wavelength. Neutral density filters were employed on the optical stimulus to keep the count rates well below saturation in the WFC3 exposures, but the total counts collected in the projected spot were of order 500,000 e^-, such that the Poisson uncertainties on the throughput measurements were of order 0.1%. The errors are thus dominated by systematics, such as the calibration of the optical stimulus.

Results

To measure the count rate incident on the WFC3 detector, aperture photometry was performed on the raw images with a local background subtraction. The aperture radius was 40 pixels, with a background annulus of radii 50 to 60 pixels. The sizes of the aperture and background annulus ensure that they enclose nearly all of the incident flux in the projected spot from the optical stimulus. Increasing or decreasing these sizes by 10 pixels has negligible effects on the calculated throughput (1% or less).

The optical stimulus calibrates the photon flux incident on the WFC3 pickoff mirror via a flux measurement on its own detectors: a photomultiplier tube for wavelengths of 600 nm or less, and a Si diode for longer wavelengths. This information is recorded in the WFC3 FITS header under the keyword "OSFLUX." The throughput, then, is just a simple ratio of the count rate (e^-/s) measured by the WFC3 CCD to the photon rate (photons/s) incident on the WFC3 pickoff mirror. This is the raw throughput, which is the desired quantity for calibrating the instrument, because it allows the observer to calculate the incident photon flux for a given count rate on the detector. However, for wavelengths shorter than 339.68 nm, there is a finite probability that a photon yields more than one electron on the CCD, due to quantum effects. These multiple electrons do not reflect an actual increase in quantum efficiency, and so it is customary to show the throughput with a "quantum-yield correction" at short wavelengths. This quantum-yield corrected throughput is not the quantity needed for converting detected count rates to incident photon flux, but it is required for a proper understanding of the statistical errors in an observation, analogous to the proper handling of detector gain. The quantum yield correction is simply the ratio of the wavelength (λ) to the critical wavelength (λ_c = 339.68 nm) for wavelengths shorter than the critical wavelength, and unity at longer wavelengths. For example, a raw QE of 0.64 at 300 nm implies a quantum-yield corrected QE of 0.57.

Note that the 200 micron UV fiber, which provides the optical stimulus flux at wavelengths of 700 nm and shorter (see Tables 1 - 3), was partially blocked within the stimulus;

the VISIR fiber was not blocked (Figure 1). Because the statistical errors with an unblocked fiber are already much less than 1%, the suppression of flux was unimportant as far as the Poisson uncertainties are concerned. Furthermore, because the flux calibration provided by the optical stimulus views the same blocked fiber as viewed by WFC3, the blocking of the UV fiber did not adversely affect the accuracy of the throughput measurements.

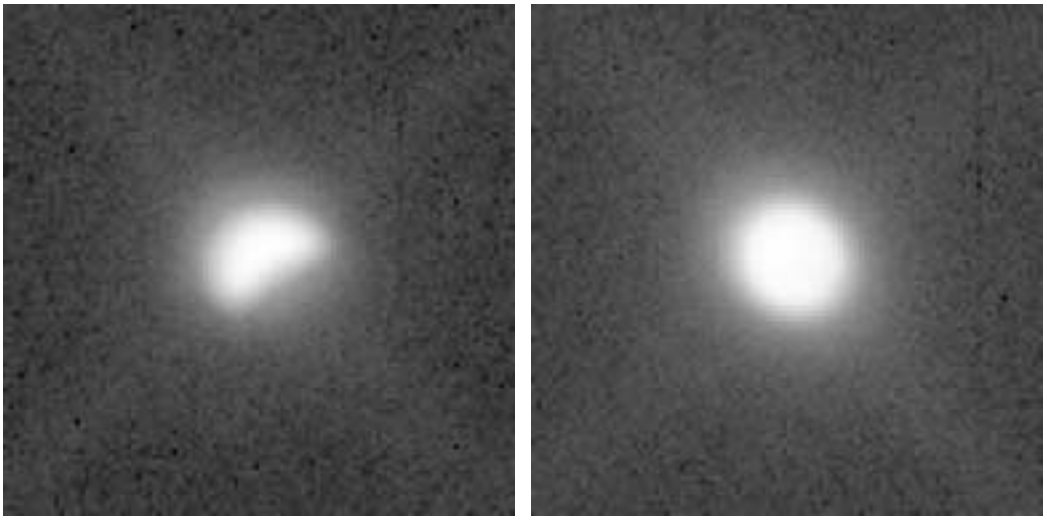

Figure 1: Images of the 200 micron UV fiber (left) and 200 micron VISIR fiber (right) on the optical stimulus, shown as 100x100 pixel subarrays on the WFC3 CCD. Note that the UV fiber was partially blocked, but this did not preclude measurements with high signal-to-noise ratio, nor did it bias the throughput measurements at short wavelengths.

The expected throughput is a product of the individual WFC3 component throughputs, as measured prior to WFC3 assembly. Those components are (Figure 2): the pick-off mirror (POM), UV mirror 1 (UVM1), UV mirror 2 (UVM2), inner window (IWIN), outer window (OWIN), detector quantum efficiency (QE; chip-dependent), and the filter transmission (F606W shown here).

Tests were repeated several times throughout the thermal vacuum program, giving a sense of the repeatability of the measurements, and also accounting for loss of data due to test anomalies. These were usually due to hardware and software errors associated with the optical stimulus, which would put the stimulus in the incorrect state (ND filter, lamp settings, etc.), although there were also occasions when a test was aborted after the first few measurements, for troubleshooting. Although these data were taken as part of the thermal vacuum program, some of the test runs were actually run under ambient conditions before WFC3 entered vacuum (5 Sep 2004) or after it emerged from vacuum (17 Oct 2004), with no noticeable difference in throughput. Tables 3 and 4 give the results of the clear throughput tests on chips 1 and 2, respectively. Table 5 gives the results of the filtered throughput tests on chip 2 (i.e., the entire WFC3 system throughput including the filtered

or clear aperture). Because the filtered throughput tests involved pairs of measurements at each wavelength (both with the filter of interest and the clear aperture), the clear measurements in Table 5 provide additional information about the clear throughput on chip 2 at wavelengths not included in Table 4. Note that, when data were not available at a given wavelength, either due to problems with the optical stimulus or aborting the test, the entry "NA" appears in Tables 3-5.

Figure 3 gives the clear WFC3 raw throughput on chip 1, as measured during thermal vacuum testing. Figure 4 gives the quantum-yield corrected throughput for chip 1 (same as Figure 3, but scaled by λ/λ_c for $\lambda<\lambda_c$). Figure 5 gives the ratio of the observed throughput to the throughput expected from the product of the component measurements (Figure 2). Figures 6 through 8 give the analogous information for chip 2, which has a significantly different QE, especially at short wavelengths (Figure 2). The throughputs are generally much higher than expected at short wavelengths; members of the Detector Characterization Lab (DCL) at GSFC now believe that the detector QE was grossly underestimated at these wavelengths. At 1000 nm, the throughput is again much higher than expected, but it is expected to be very low, so the doubling of the throughput does not result in a useful throughput at such long wavelengths. The QE was measured by DCL with a normal-incidence beam, unlike the non-normal incidence (20^o) of the beam hitting the detector when integrated into WFC3; the non-normal incidence increases the path length through the CCD substrate, increasing the QE at long wavelengths.

Figure 9 shows the measured filter transmissions from Table 5, taking the ratio of the filtered throughput measurement to the clear throughput measurement for the pair of measurements made at the central wavelength of each filter tested. Figure 10 compares these filter transmissions to the expected transmission at each central wavelength, again using the data from Table 5. The filter transmissions are systematically low at the shortest wavelengths, possibly indicating degradation or contamination of these filters. Most of the remaining filters are near their expected values, but the F775W shows a higher-than-expected transmission. Figure 11 shows the total WFC3 throughput (filter + system) at the central wavelength of each filter tested, as compared to expectations. Here, the low filter transmission at the shortest wavelengths is compensated by the better-than-expected detector QE, such that the total throughput is higher than expected.

To look for any time evolution in the short-wavelength throughput, Figures 9 and 10 also show data from the "mini-calibration" tests of Jan 2004 (made with the F218W filter but not at the central wavelength of 218 nm). Reid et al. (2004, ISR WFC3-2004-05) first characterized the UVIS throughput with these data, under ambient conditions, although it is worth noting that the test procedures and the calibration of the optical stimulus have both been updated since then. The mini-calibration data also show a transmission deficit, compared to expectations, but it is not as significant as that seen during the tests in the fall of 2004, suggesting that the throughput of the F218W filter has indeed declined with time. Two more data points are available from the "UV Science Monitor" taken during ambient

tests on 9 Jul 2004; these two images were obtained in a manner similar to the throughput tests of the thermal-vacuum program, except that the subarrays were only 512x512 pixels, the bandpass was 13 nm instead of 10 nm, and measurements were taken only through the F218W filter at 218 nm, with no corresponding measurement through the clear aperture. These two images gave raw filtered throughputs of 0.11 and 0.16, compared to two measurements of 0.15 in the thermal-vacuum tests in Sep and Oct 2004 (Table 5); given the differences in the configuration between the summer ambient test and the fall thermal-vacuum tests, the measurements in the summer and fall are consistent. The lever on time evolution between the summer and fall is probably too small to indicate whether or not the throughput of the F218W filter declined beyond the date of the summer tests.

Summary

Overall, the WFC3 UVIS channel shows excellent throughput across a wide wavelength range, meeting or exceeding expectations at most wavelengths. The filter transmission at the shortest wavelengths is somewhat lower than expected, possibly indicating filter degradation or contamination, but at the current time the diminished filter transmission is offset by the better-than-expected detector QE at those wavelengths.

Table 3: Clear WFC3 throughput on chip 1

wavelength (nm)	raw throughput 30 Aug 2004	raw throughput 31 Aug 2004	raw throughput 30 Sep 2004	raw throughput 20 Oct 2004	expected throughput
200	0.17	0.17	0.17	0.17	0.20
205	0.21	0.21	0.21	0.21	0.22
210	0.26	0.26	0.26	0.26	0.25
215	0.31	0.30	0.30	0.30	0.27
220	0.33	0.33	0.34	0.34	0.29
225	0.37	0.37	0.37	0.37	0.33
230	0.41	0.41	0.41	0.41	0.36
235	0.44	0.43	0.43	0.43	0.39
240	0.44	0.44	0.43	0.44	0.42
245	0.44	0.43	0.43	0.44	0.42
250	0.44	0.43	0.43	0.43	0.42
255	0.41	0.41	0.41	0.41	0.41
260	0.40	0.40	0.39	0.40	0.41
270	0.36	0.36	0.35	0.36	0.39
280	0.36	0.36	0.33	0.34	0.41
290	0.35	0.35	0.34	0.35	0.44
300	0.37	0.37	0.35	0.36	0.46
320	0.37	NA	0.36	0.36	0.43
340	0.35	NA	0.34	0.34	0.40
360	0.31	NA	0.30	0.30	0.36
380	0.33	NA	0.33	0.33	0.35
400	0.38	NA	0.37	0.37	0.38
450	0.41	NA	0.41	0.40	0.41
500	0.42	NA	0.42	0.41	0.43
550	0.44	NA	0.44	0.43	0.43
600	0.44	NA	0.44	0.44	0.43
650	0.39	NA	0.40	0.40	0.42
700	0.39	NA	0.36	0.36	0.37
750	0.32	NA	0.33	0.31	0.32
800	NA	NA	0.25	0.25	0.27
850	NA	NA	NA	0.21	0.21
900	NA	NA	0.15	0.16	0.16
950	NA	NA	0.09	0.10	0.11
1000	0.04	NA	0.04	0.04	0.02

Table 4: Clear WFC3 throughput on chip 2

wavelength (nm)	raw throughput 8 Jul 2004	raw throughput 31 Aug 2004	raw throughput 2 Oct 2004	expected throughput
200	0.23	0.23	0.24	0.23
205	0.30	0.30	0.30	0.26
210	0.37	0.37	0.39	0.29
215	0.43	0.43	0.45	0.32
220	0.48	0.48	0.50	0.36
225	0.52	0.53	0.54	0.40
230	0.57	0.57	0.58	0.44
235	0.58	0.59	0.60	0.48
240	0.57	0.57	0.59	0.51
245	0.56	0.56	0.58	0.50
250	0.54	0.54	0.55	0.49
255	0.50	0.50	0.51	0.47
260	0.47	0.47	0.48	0.45
270	0.40	0.40	0.41	0.41
280	0.38	0.38	0.39	0.41
290	0.39	0.40	0.41	0.43
300	0.41	0.41	0.42	0.45
320	0.41	NA	0.41	0.43
340	0.39	NA	0.39	0.40
360	0.34	NA	0.34	0.35
380	0.35	NA	0.36	0.35
400	0.38	NA	0.39	0.39
450	0.40	NA	0.40	0.42
500	0.41	NA	0.41	0.44
550	0.42	NA	0.43	0.44
600	0.42	NA	0.43	0.44
650	NA	NA	NA	0.44
700	NA	NA	0.36	0.42
750	NA	NA	0.30	0.38
800	NA	NA	0.25	0.31
850	NA	NA	0.18	0.25
900	NA	NA	0.15	0.20
950	NA	NA	0.09	0.10
1000	NA	NA	0.04	0.02

Table 5: Filtered WFC3 throughput on chip 2

WFC3 filter[a]	raw throughput 19 Sep 04	raw throughput 30 Sep 04	raw throughput 3 Oct 04	expected throughput
F218W	0.15	NA	0.15	0.12
CLEAR	0.51	NA	0.51	0.34
F225W	0.14	0.14	0.14	0.12
CLEAR	0.57	0.56	0.57	0.40
F275W	0.13	0.12	0.13	0.13
CLEAR	0.39	0.39	0.39	0.41
F300X	0.14	0.14	0.14	0.14
CLEAR	0.42	0.42	0.42	0.45
F336W	0.30	0.30	0.30	0.30
CLEAR	0.40	0.40	0.40	0.41
F390W	0.36	0.36	0.36	0.35
CLEAR	0.38	0.38	0.38	0.37
F438W	0.33	0.34	0.34	0.33
CLEAR	0.41	0.40	0.41	0.41
F475X	0.39	0.38	0.38	0.40
CLEAR	0.41	0.41	0.41	0.43
F475W	0.37	0.37	0.37	0.38
CLEAR	0.41	0.41	0.41	0.43
F555W	0.38	0.38	0.37	0.38
CLEAR	0.43	0.43	0.43	0.44
F606W	NA	0.38	0.37	0.41
CLEAR	NA	0.40	0.39	0.44
F625W	0.35	0.36	0.36	0.39
CLEAR	0.39	0.40	0.39	0.43
F775W	0.26	0.26	0.26	0.23
CLEAR	0.28	0.27	0.28	0.28
F814W	0.23	0.22	0.23	0.22
CLEAR	0.25	0.24	0.23	0.23

a. Note that the optical stimulus was set to the central wavelength of the filter for the exposure through the filter and the subsequent exposure taken through the clear aperture. For example, the first two exposures were taken at 218 nm, the next two at 225 nm, etc.

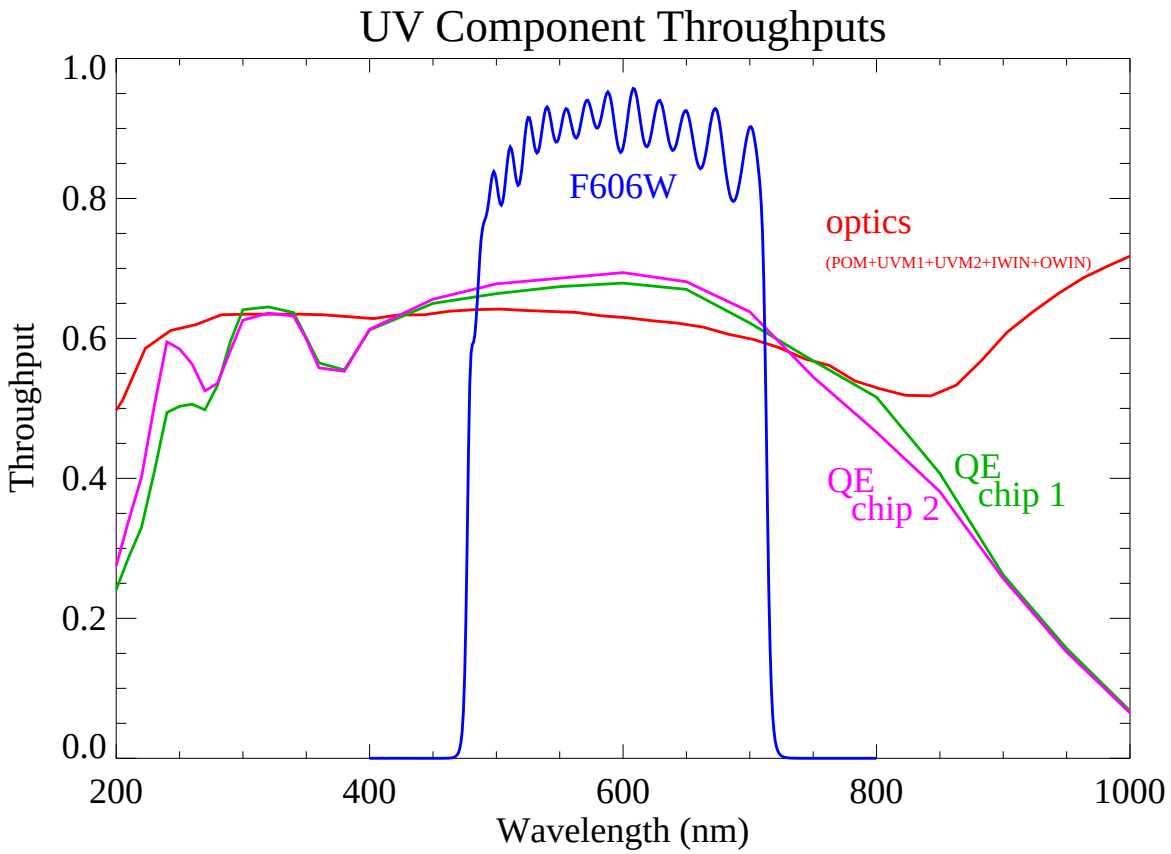

Figure 2: The component throughputs for the UVIS channel, along with the filter transmission of the F606W filter. It is now thought that the short-wavelength QE was significantly underestimated during component testing.

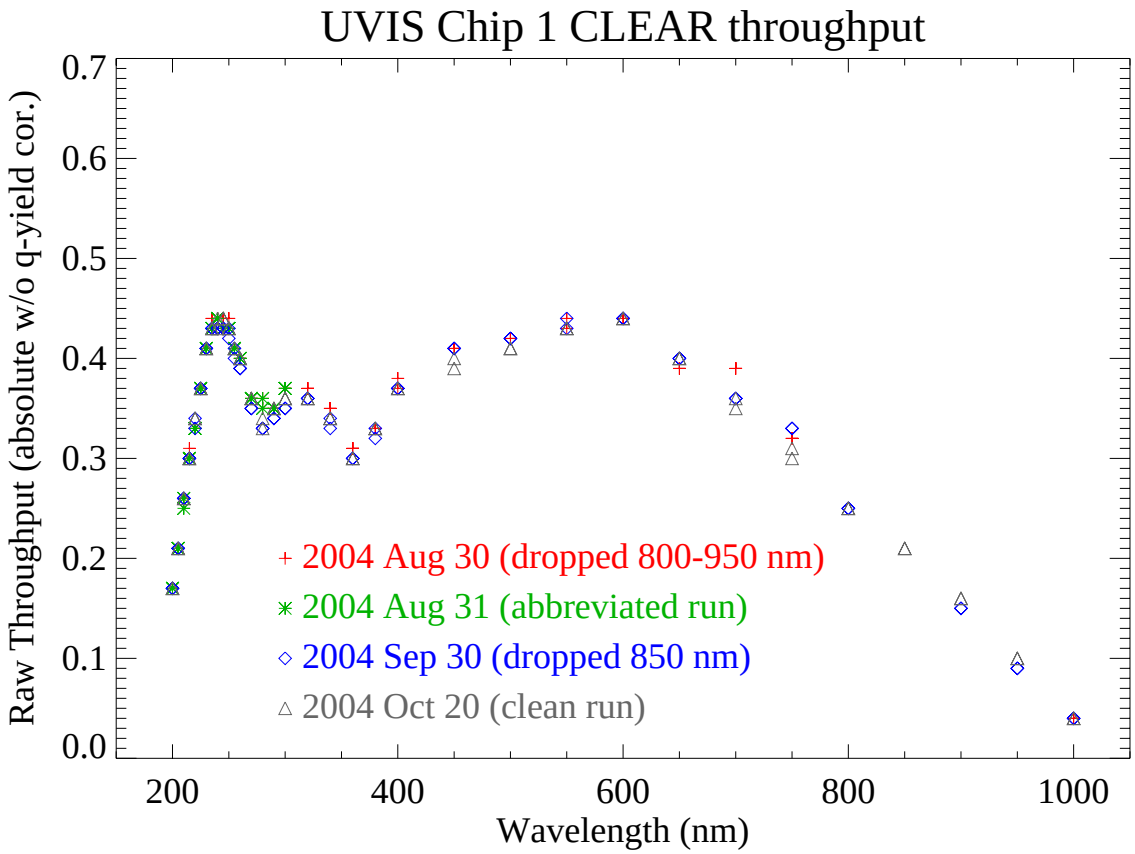

Figure 3: The raw throughput for the clear aperture on the WFC3 UVIS channel (no quantum-yield correction), as observed on chip 1.

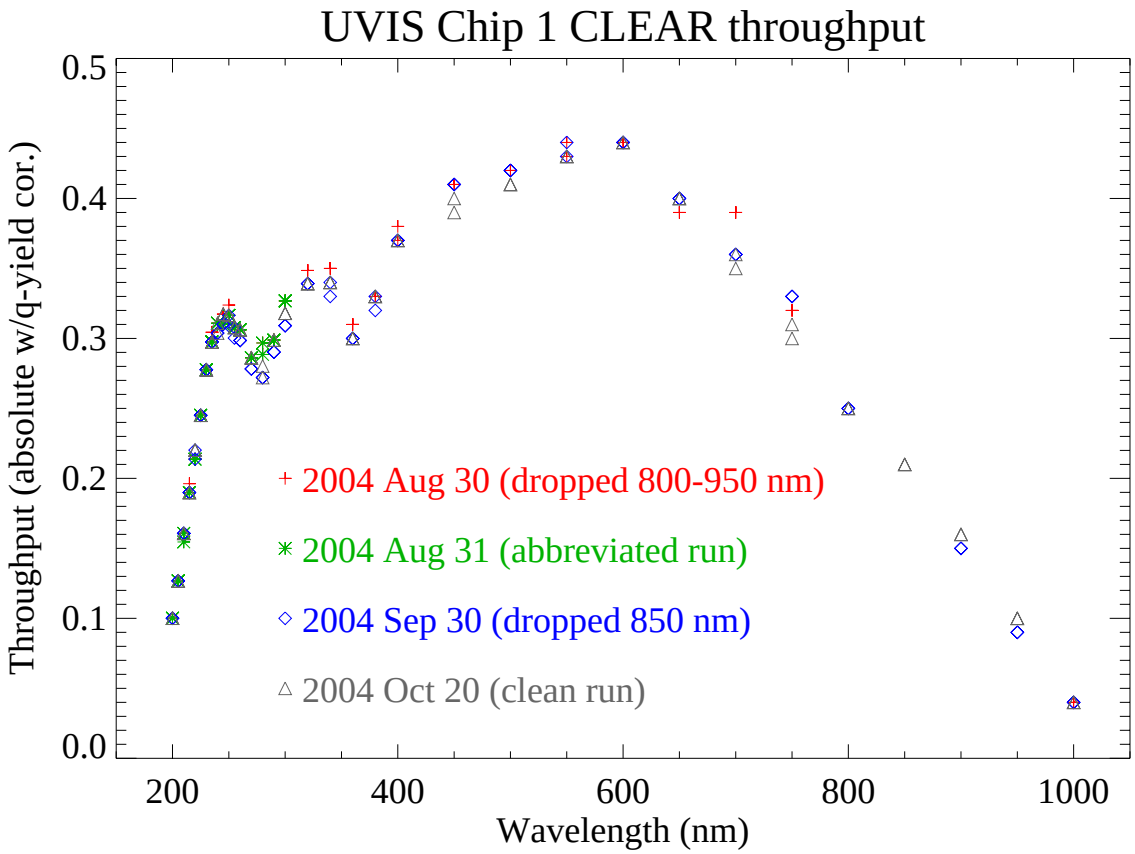

Figure 4: The same as Figure 3, but with a correction for the quantum effects at wavelengths shorter than 339.68 nm.

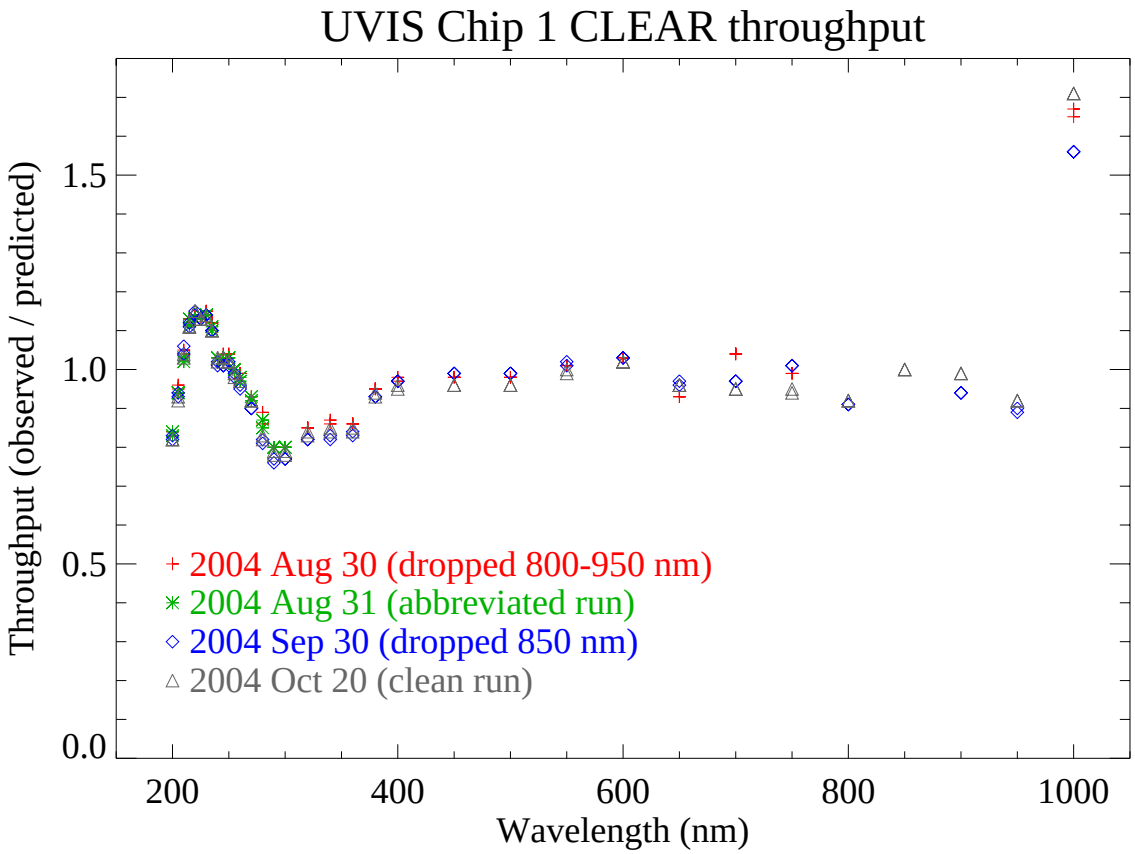

Figure 5: The ratio of the measured chip 1 throughput to the expected throughput (based upon the component measurements).

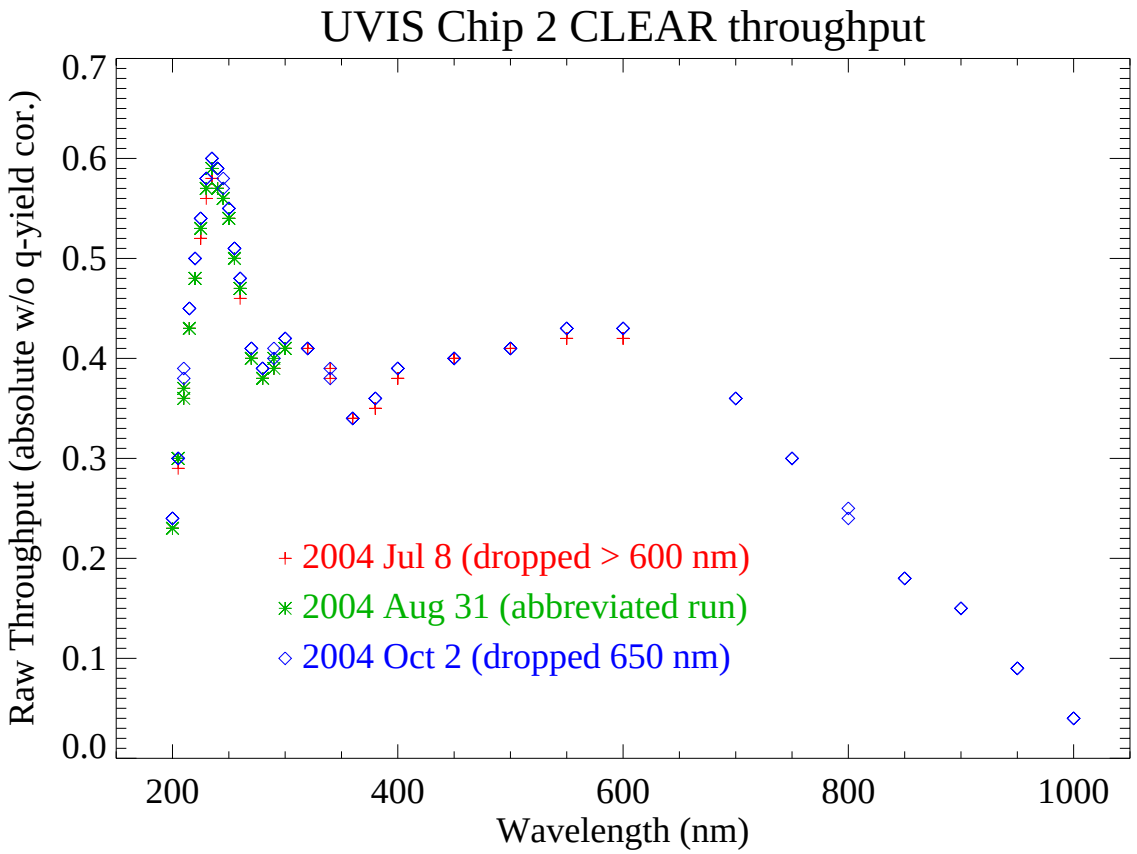

Figure 6: The raw throughput for the clear aperture on the WFC3 UVIS channel (no quantum-yield correction), as observed on chip 2.

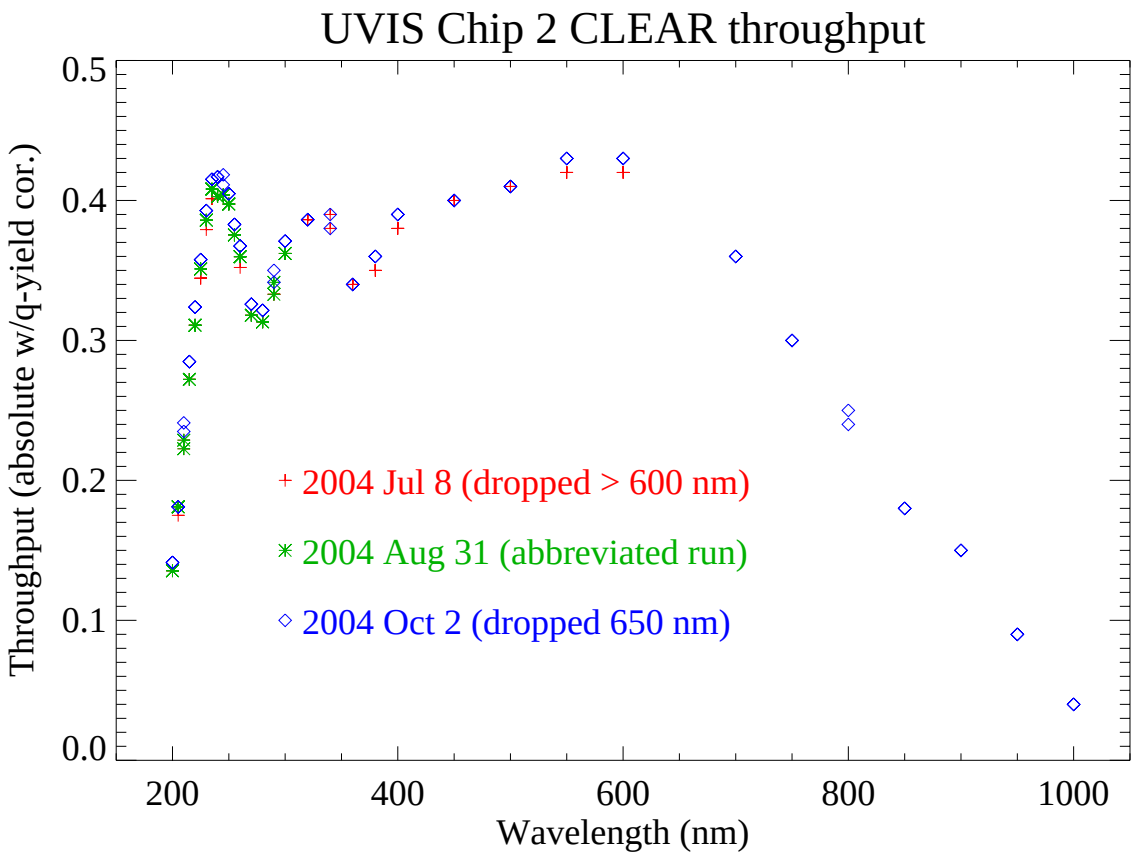

Figure 7: The same as Figure 6, but with a correction for the quantum effects at wavelengths shorter than 339.68 nm.

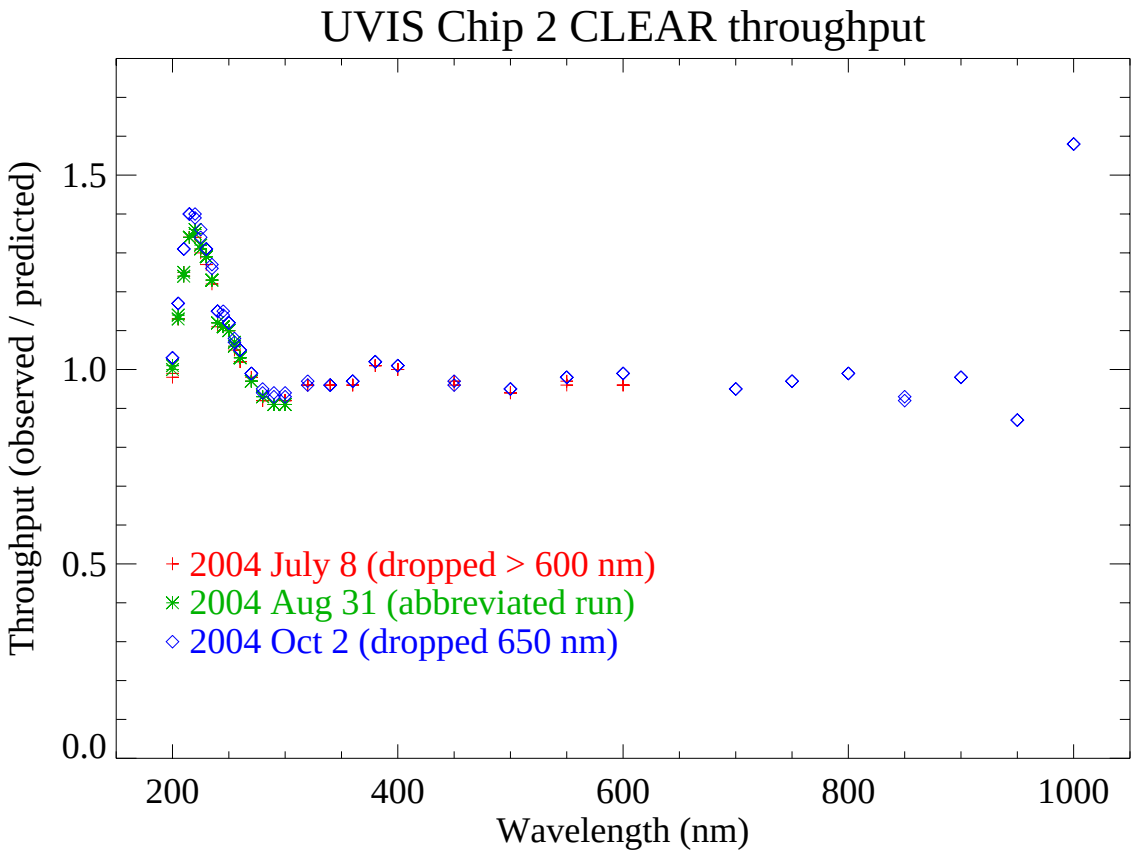

Figure 8: The ratio of the measured chip 2 throughput to the expected throughput (based upon the component measurements).

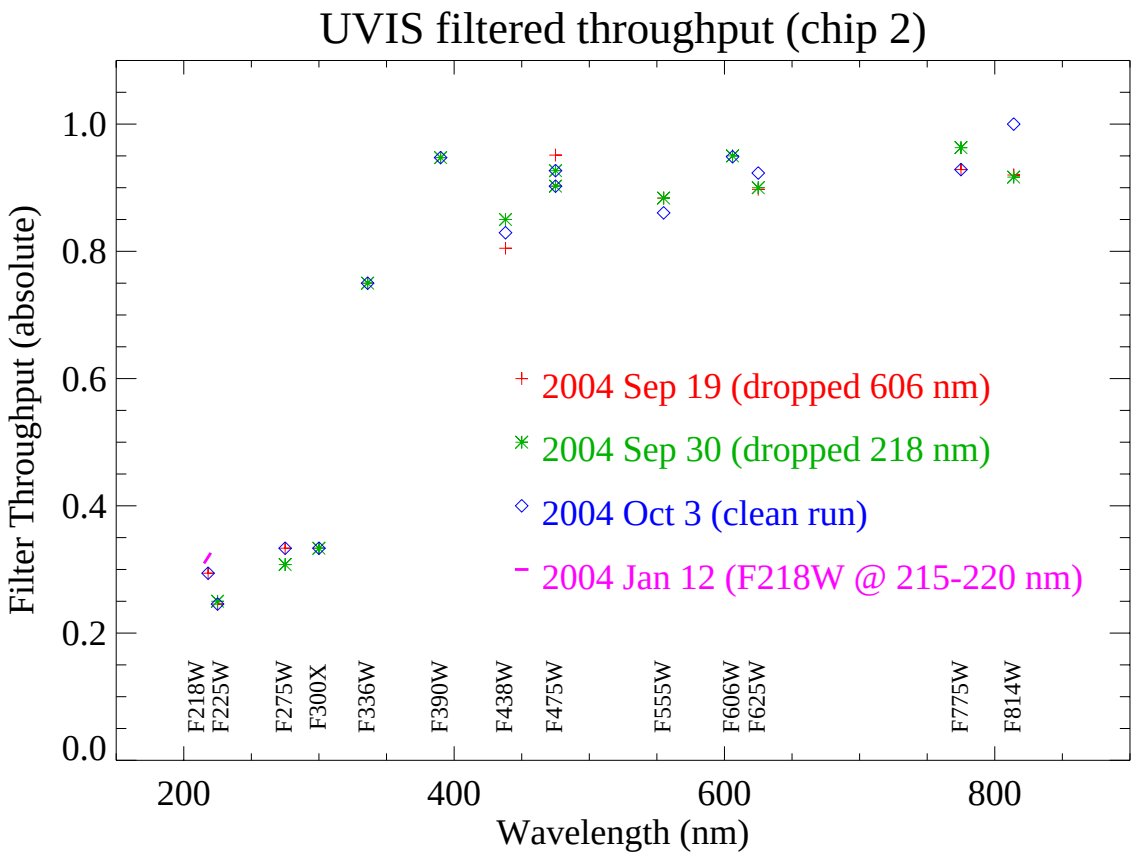

Figure 9: The transmission at the central wavelengths for a subset of the UVIS filters, as measured on chip 2. Because this is simply the ratio of the filtered throughput to the clear throughput at each wavelength (taking pairs of measurements from Table 5), no quantum-yield correction is necessary. For comparison, data from the F218W measurements of Jan 2004 are also shown.

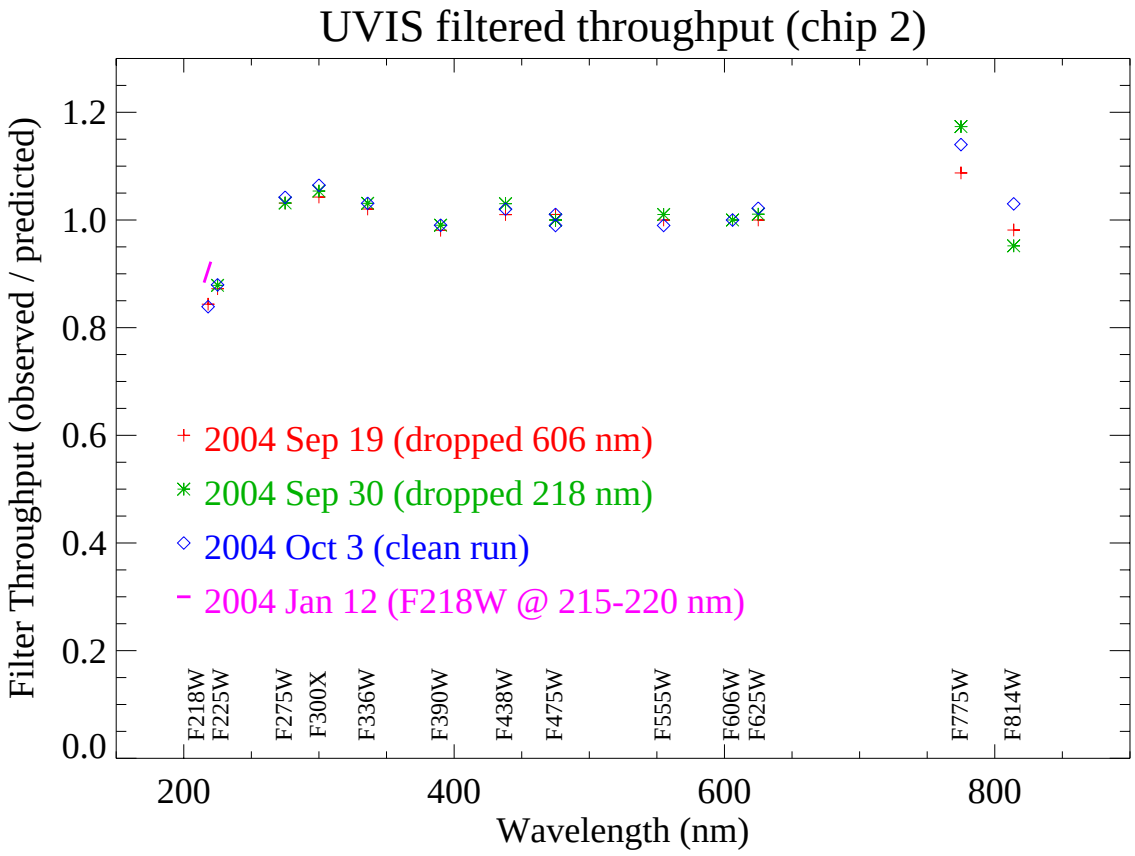

Figure 10: The filter transmission (taking the pairs of measurements at each wavelength in Table 5), compared to the expected transmission from measurements made before the filters were integrated into WFC3.

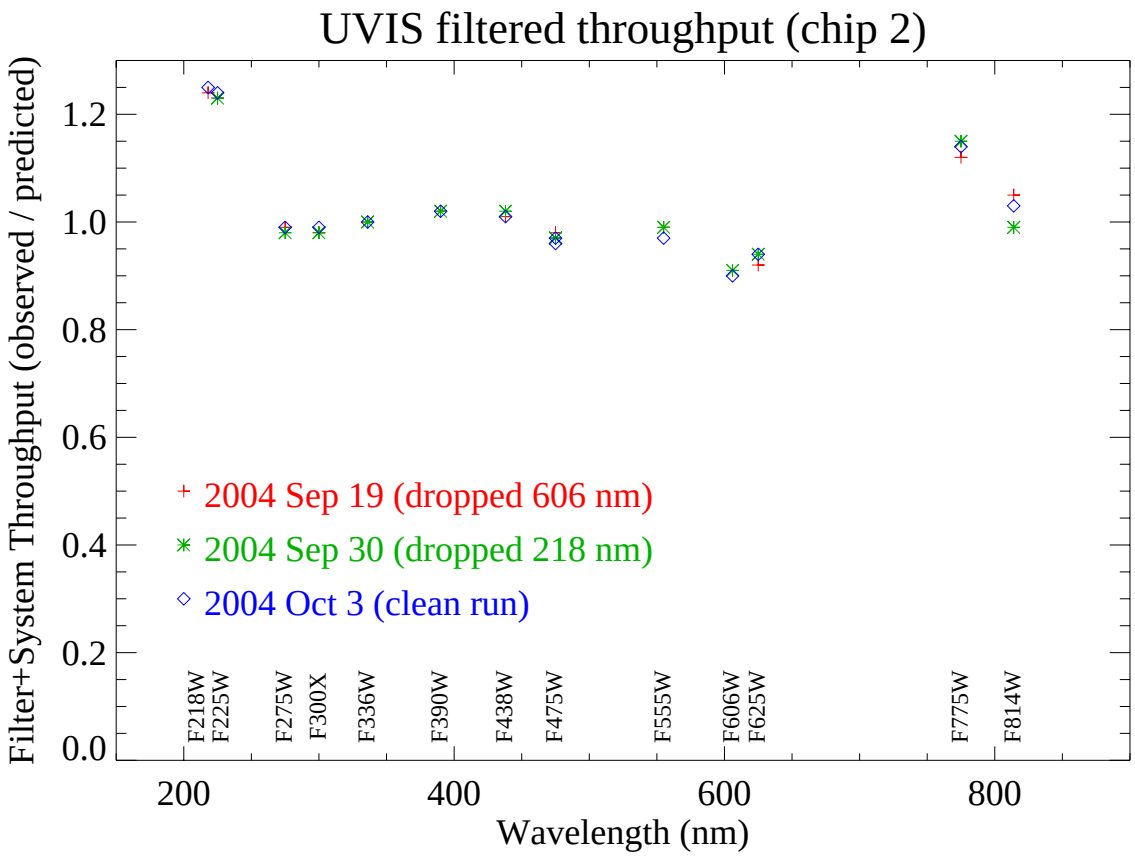

Figure 11: The total WFC3 throughput, as observed at the central wavelengths for a subset of the UVIS filters, compared to the expected throughput (both taken directly from Table 5). The loss of filter transmission at the shortest wavelengths is offset by the better-than-expected QE of the detector at these wavelengths.